A Sensitive Skin Based on Touch-Area-Evaluating Tactile Elements

Takayuki Hoshi* Hiroyuki Shinoda†

The University of Tokyo

ABSTRACT

In this paper, we propose a new tactile sensor skin system. The system consists of two components. One is a sensor element which detects a contact area in addition to a contact force. The element is inspired by the fact that humans can discriminate sharpness of objects sensitively on any parts of their bodies in spite of their several-cm Two Point Discrimination Thresholds. We have developed the element that has such characteristics in a very simple structure; two layers of compressible insulators (urethane foam) sandwiched between three pieces of stretchable conductive sheets (conductive fabric). The other component is a sensor/communication chip. The chips are arranged at the boundaries of the elements, and the chips measure the capacitances between the conductive layers and send signals through the same conductive layers. The chips enable us to connect the elements and compose a soft robot skin including no long wires.

CR Categories: I.2.9 [Artificial Intelligence]: Robotics—Sensors

Keywords: Tactile sensor, Artificial skin, Robot skin, Haptic interface, Contact area, Nonlinear elasticity

1 INTRODUCTION

Realizing an elastic senor skin to provide sufficient contact information is one of classical and unsolved problems in haptics. Recently, there is a growing interest in home robots that can care for the aged and young children [1, 2] and that can be alternatives to companion animals [4, 3]. A skin covering such a robot is in an urgent need. The skin is not only a device for autonomous motions of a robot but also a new form of interface between humans and artificial systems [5].

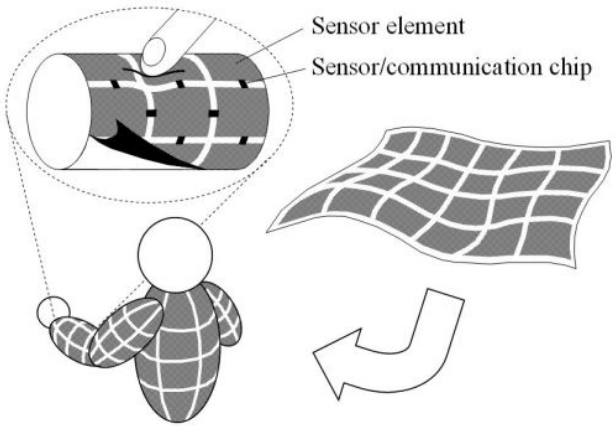

Figure 1: Proposed tactile sensor skin system. It is soft, stretchable, and capable to cover a large area easily.

The major requirements for practical robot skins are as follows.

- They should sensitively detect rich tactile information related to such parameters as shape, pressure, friction, temperature, and so on.
- They should cover several-cm^2 large areas such as whole surfaces of robots.
- They should be soft and stretchable to contact humans safely and fit robot surfaces. Softness is one of important factors to detect touch feelings, too.

In order to realize such a robot skin, various arrays of pressure-sensitive tactile sensor elements have been tried [6, 7, 8, 9, 10, 11]. One approach to enhance the ability of the sensors for practical uses is to array the elements in high density. However, we have no practical techniques available now with which we can mount a million of tactile elements with 1 mm spacing in a stretchable sensor skin.

We have proposed a new tactile sensing method to solve the problem [12]. In our method, a sensor element dares to have a large sensing area (several cm^2) unlike the other elements in the literature, and it acquires not only a contact force but also a contact area. Owing to the additional parameter, the contact area, a robot skin which detects minute shape features is easily realized by arraying the elements in low density. In consequence, we can cover a whole surface of a robot with a small amount of the elements (Fig.1).

The above proposition is inspired by the characteristics of the human tactile sensation. While Two Point Discrimination Thresholds (TPDT) of humans are as large as several cm except on especially sensitive parts, faces and hands, humans can discriminate sensitively sharpness of objects even on such large TPDT parts. Although we still don't know exactly why and how the human skins perform like that, from these facts, we consider that sharpness is one of key components to produce general human tactile sensation [13], and suppose that sensitivity to sharpness is a high priority for human-like sensor skins.

Based on the proposition, we developed a new tactile sensor element [12]. The element consists of two layers of compressible insulators and three pieces of stretchable conductive sheets. In order to acquire the contact force and the contact area, we make use of the nonlinear elasticity of the insulators.

In this paper, we also present a connecting method well suited to the tactile elements. In the method, the conductive pieces work not only as sensor elements but also as communication paths when sensor/communication chips are placed at the boundaries of the conductive pieces [14]. Thus, wires to the sensor elements are no longer needed and stretchable skins can be realized.

The rest of this paper is organized as follows. Firstly, section 2 describes the structure and the sensing theory of the sensor element. We show results of experiments examining the feasibility of the element. After that, we explain about the proposed sensor skin system in section 3. Developed CMOS LSI chips for connecting the sensor elements without long wires are introduced.

*e-mail: star@alab.t.u-tokyo.ac.jp
†e-mail: shino@alab.t.u-tokyo.ac.jp

Symposium on Haptic Interfaces for
Virtual Environment and Teleoperator Systems 2006
March 25 - 26, Alexandria, Virginia, USA
1-4244-0226-3/06/$20.00 ©2006 IEEE

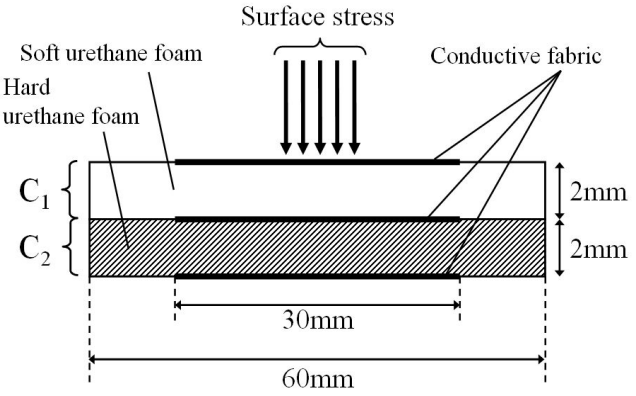

Figure 2: Cross-section of sensor element prototype.

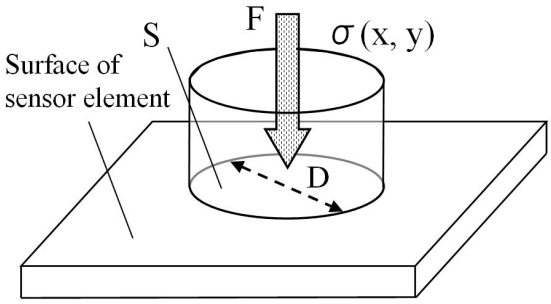

Figure 3: Supposed surface stress distribution.

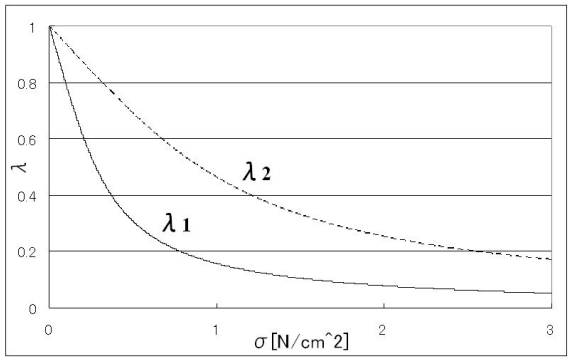

Figure 4: Relationship between surface stress and extension ratio. Soft layer 1 is more easily compressed than hard layer 2.

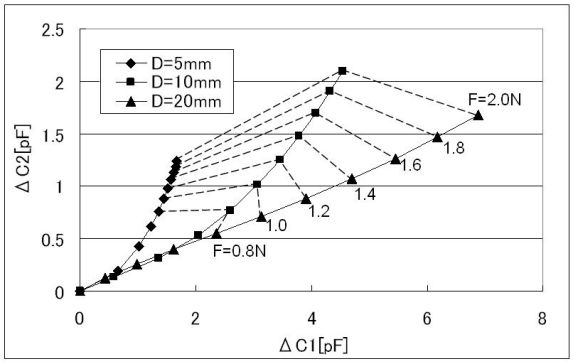

Figure 5: Simulation result. Calculated capacitance variations for various forces and areas. D is the diameter of S for a circular object.

2 Sensor element

2.1 Structure

The structure of our sensor element is very simple. In Fig.2, we show schematically the cross-section of the sensor element prototype. The sensor element consists of two compressible insulator layers; the upper and lower layers are soft (15 kg/m^3) and hard (60 kg/m^3) urethane foam, respectively, and each layer is 2 mm in thickness. There are three pieces of stretchable conductive fabric on the soft layer, between the soft and hard, and under the hard. Each piece has an area of 30×30 mm^2. The side length of the conductive fabric piece is comparable to the TPDT on human forearms. The insulator layers and the conductive pieces adhere to each other by soft double-faced tape, and two capacitors are formed in the layers. Supposing that a surface of a robot body is hard, we attach the bottom of the sensor element prototype to an acrylic base.

2.2 Sensing theory

We suppose the surface stress as illustrated in Fig.3; the constant surface stress distribution $\sigma(x,y)$ [Pa] is vertically loaded to the surface of the sensor element in the contact field S, that is,

$$\sigma(x,y) \equiv \begin{cases} F/S & \text{if } (x,y) \in \mathrm{S} \\ 0 & \text{if } (x,y) \notin \mathrm{S} \end{cases} \tag{1}$$

where F [N] is the total intensity of the contact force and S [m^2] is the area of S. Now we take note of the area of S, not the shape, so we suppose that S is circular for simplicity.

We also assume the following. First, the nonlinear elasticity of the insulator layers is the entropy elasticity [15] expressed as

$$\sigma = \frac{E_n}{3}\left(\frac{1}{\lambda_n} - \lambda_n^2\right) \quad (n = 1,2) \tag{2}$$

$$\lambda_n \equiv \frac{d_n - \Delta d_n}{d_n} \tag{3}$$

where n is the layer identification; n=1 means the upper soft layer and 2 the lower hard layer. E_n [Pa], λ_n and d_n [m] are the elasticity modulus, the extension ratio and the initial thickness of the layer n, respectively. E_1 is 4.8 kPa and E_2 is 15 kPa. The following expression of λ_n (Fig.4) is obtained by solving Eq.(2),

$$\lambda_n = \sqrt[3]{\frac{1}{2} + \sqrt{\frac{1}{4} + \left(\frac{\sigma}{E_n}\right)^3}} + \sqrt[3]{\frac{1}{2} - \sqrt{\frac{1}{4} + \left(\frac{\sigma}{E_n}\right)^3}}. \tag{4}$$

Second, the conductive pieces have negligible tensions and the Poisson's ratios of the insulator layers are zero, which means that a displacement distribution $\Delta d_n(x,y)$ [m] is determined simply by the local value of $\sigma(x,y)$.

We measure electric capacitances C_n [F] between the conductive pieces to detect $\Delta d_n(x,y)$. Ignoring fringing fields, the capacitances are formulated as

$$C_n = \iint_{\text{Element}} \frac{\varepsilon_n}{d_n - \Delta d_n(x,y)} \mathrm{d}x\mathrm{d}y \tag{5}$$

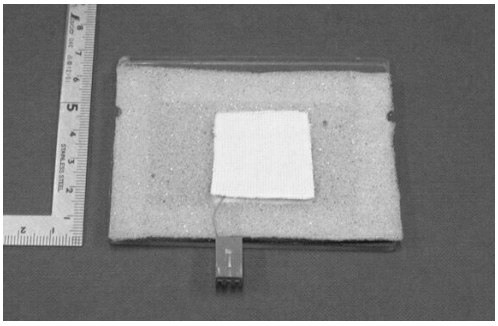

Figure 6: Photograph of sensor element prototype.

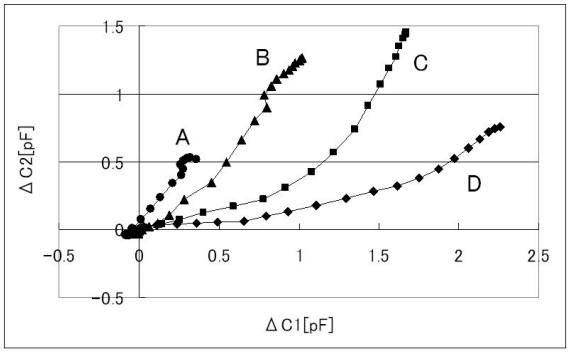

Figure 7: Experimental result of basic performance. Measured trajectories of capacitance variations for the stimulators with diameters of (A) 0.5 mm, (B) 10 mm, (C) 20 mm, and (D) 40 mm.

where ε_n [F/m] is the dielectric constant of the layer n. If we can make the second assumption mentioned above, (C_1, C_2) is uniquely determined by (F, S). Then the key question is whether the inverse mapping from (C_1, C_2) to (F, S) is possible or not for the layers, 1 and 2, having different hardness.

Figure 5 shows a numerical simulation result for the elasticity moduli E_1=4.8 kPa and E_2=15 kPa. It shows that $(\Delta C_1, \Delta C_2)$s for various (F, S)s span a two dimensional space, where $(\Delta C_1, \Delta C_2)$ are the capacitance variations by the applied force, and D [m] is the parameter defined as

$$D \equiv 2\sqrt{\frac{S}{\pi}} \tag{6}$$

to represent the diameter of S for a circular object. It implies that we can determine (F, S) uniquely from $(\Delta C_1, \Delta C_2)$ when F is larger than a threshold, now around 1.0 N.

Note that the nonlinear elasticity of the insulator layers plays a key role in the sensing theory. In the case of linear elastic insulator layers, that is, $\sigma \ll E_n$, it is impossible to estimate S from (C_1, C_2). $\Delta d_n(x, y)$ of the linear elastic insulator is represented as

$$\Delta d_n(x, y) = \frac{d_n}{E_n}\sigma. \tag{7}$$

Then Eq.(5) can be approximated as

$$C_n \simeq C_{n0} + \frac{\varepsilon_n}{d_n E_n} F \tag{8}$$

where C_{n0} is the initial capacitance of the layer n. Eq.(8) means that neither C_1 nor C_2 contains the parameter S.

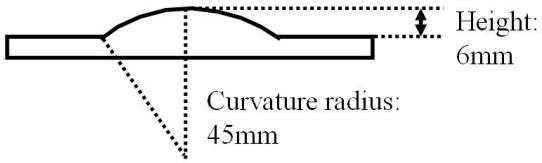

Figure 8: Base with hemispherical bump.

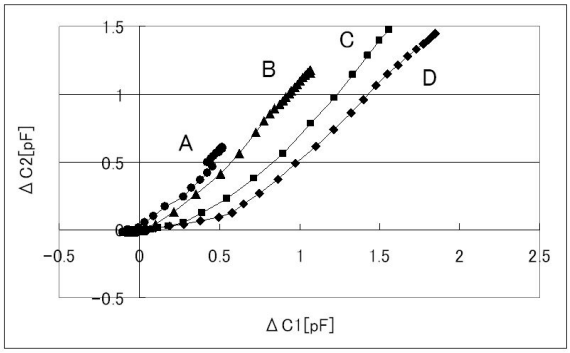

Figure 9: Experimental result on effect of surface configuration. Measured trajectories of capacitance variations for the stimulators with diameters of (A) 0.5 mm, (B) 10 mm, (C) 20 mm, and (D) 40 mm.

2.3 Experiments and results

We conducted experiments to examine the feasibility of the proposed sensing method. We measured C_n of a sensor element prototype (Fig.6) by a self oscillation method; we generated a RC oscillation including the sensor element as the capacitor, and counted pulses par 2 ms by a 16-bit counter. A PC imported data via a digital I/O, and achieved around 80 Hz effective sampling rate.

2.3.1 Basic performance

This experiment examined whether the sensor element prototype could discriminate four different acrylic-circular-cylinder stimulators; A: D=0.5 mm (as a concentrated load), B: D=10 mm, C: D=20 mm, and D: D=40 mm (as a whole-area load). Each stimulator was vertically pressed at the center of the sensor element by hand with increasing force up to around 10 N in 0.5 s. Then the values of ΔC_1 and ΔC_2 increased with the contact force.

In Fig.7, the $(\Delta C_1, \Delta C_2)$s during the motion are plotted. It is confirmed possible to discriminate the four stimulators.

2.3.2 Effect of surface configuration

A robot surface to which the sensor skin is attached is not always flat. This experiment examined whether the prototype could discriminate the four stimulators A, B, C, and D even when it was placed on the base with the hemispherical bump shown in Fig.8. As in Section 2.3.1, each stimulator was vertically pressed at the center of the sensor element by hand with increasing force up to around 10 N in 0.5 s.

In Fig.9, the $(\Delta C_1, \Delta C_2)$s during the motion are plotted. It is confirmed possible to discriminate the four stimulators when the sensor element is attached to the curved surface.

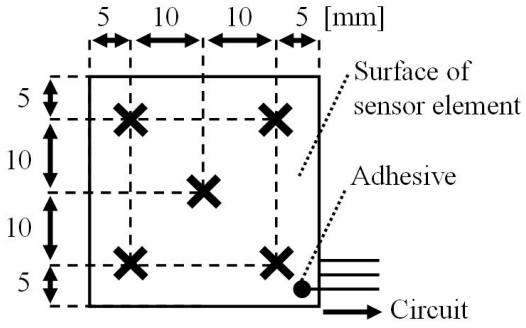

Figure 10: Pressed positions; the center and the four corners.

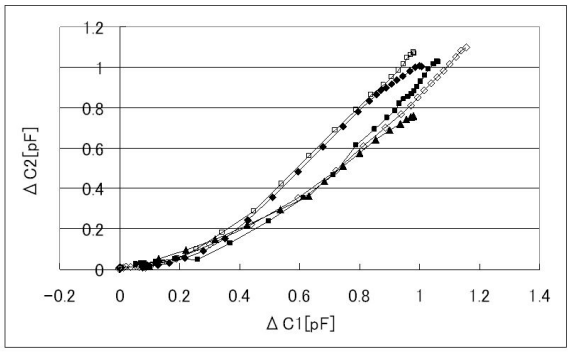

Figure 11: Experimental result on effect of contact position. Measured trajectory of capacitance variations for the stimulator with a diameter of 10 mm.

2.3.3 Effect of contact position

The sensitivity of the sensor element is not affected by contact positions because C_n is a spatial integration value. This experiment examined whether the outputs of the prototype had some relationship with the contact positions on the surface of the prototype. We pressed the center and the corners of the sensor element as illustrated in Fig.10 by the stimulator B. The other conditions were the same as the experiment in Section 2.3.1.

In Fig.11, the $(\Delta C_1, \Delta C_2)$s during the motion are plotted. It is confirmed that the maximal deviation is about 0.2 pF and sufficiently small.

2.3.4 Effect of force direction

The sensor element is not sensitive to forces which are parallel to the surface of the element because only normal forces affect the distance between the conductive pieces. This experiment examined whether the outputs of the prototype had some relationship with the force direction, i.e. the existence of the surface shear stress. We pressed the center of the sensor element by the stimulator A not only vertically but also aslope at angles of $\pm 45^\circ$ from the vertical line. The other conditions were the same as the experiment in Section 2.3.1.

In Fig.12, the $(\Delta C_1, \Delta C_2)$s during the motion are plotted. It is confirmed that the maximal deviation is about 0.1 pF and sufficiently small.

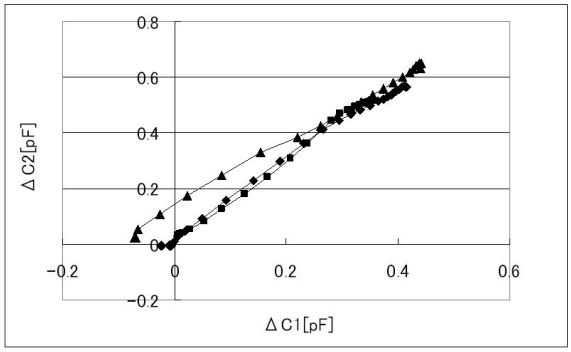

Figure 12: Experimental result on effect of force direction (-45°, 0°, and 45°). Measured trajectory of capacitance variations for the stimulator with a diameter of 0.5 mm.

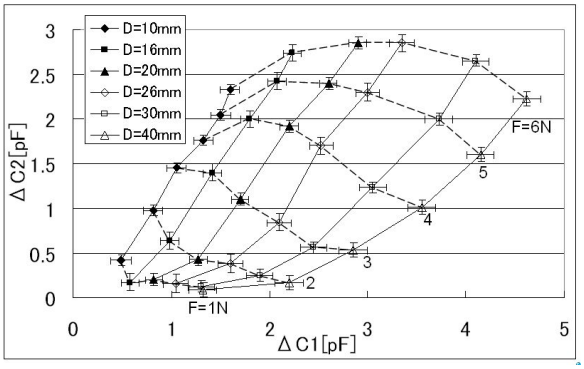

Figure 13: Experimental result on reproducibility. Measured capacitance variations for forces and contact diameters with error bars representing the maximal deviations.

2.3.5 Reproducibility of results

This experiment examined whether the outputs of the prototype were reproducible. We used the six acrylic-circular-cylinder stimulators with diameters D=10 mm, 16 mm, 20 mm, 26 mm, 30 mm, and 40 mm. Each stimulator was vertically pressed at the center of the sensor element quasi-statically by a mechanical setup (a z-stage) measuring the pressing force. This setup is for more detailed data than the previous experiments, especially about the force.

In Fig.13, the averaged $(\Delta C_1, \Delta C_2)$s of the five trials are plotted with the error bars representing the maximal deviations. It is confirmed that the outputs were stable during the five trials.

2.3.6 Effect of hysteresis

Figures 7, 9, 11, and 12 are the plots of $(\Delta C_1, \Delta C_2)$ during loading sequences. Actually, there is a relaxation stage of the insulator layers after lifting off the stimulators and it is observed as a hysteresis (Fig.14). While the hysteresis leads to estimation errors, the effect is as small as 0.2 pF at the maximum and finishes sooner than 1 s.

3 SENSOR SKIN SYSTEM

3.1 Structure

We are developing a sensor/communication chip that measures the capacitance C_n and transmits signals to the host computer without

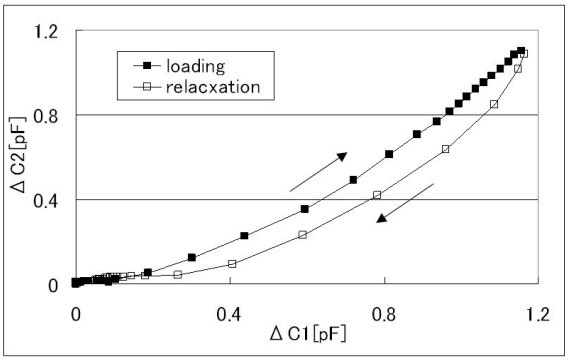

Figure 14: Experimental result of hysteresis. Measured trajectory of capacitance variations for the stimulator with a diameter of 10 mm.

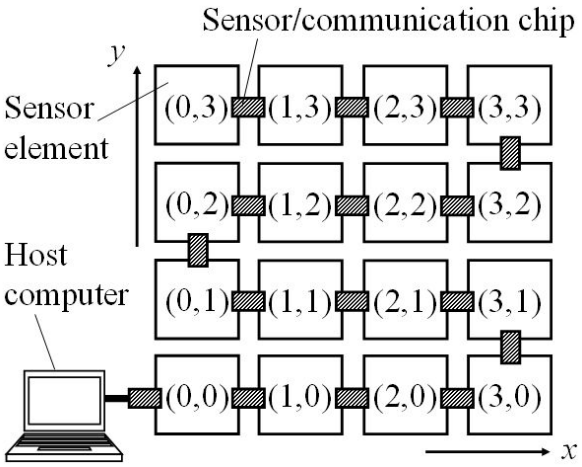

Figure 15: Scheme of sensor skin. Each sensor element has its specific coordinate as shown in the figure.

long wires. Eliminating long wires is crucial to realize a practical elastic sensor skin. In our method, we use the conductive pieces of the sensor elements also for signal transmission.

The scheme of the sensor skin system is illustrated in Fig.15. The system consists of the arrayed sensor elements and the sensing chips arranged at the boundaries of the sensor elements. While we will arrange the bridges at all four sides of the sensor elements in future, we now connect the elements in a row for simplicity of the protocol. Each sensor element has its specific coordinate as shown in Fig.15. The element with the coordinate $(0,3)$ is the most upstream, and the element with $(0,0)$ is the most downstream connected to the host computer. While the number of the sensor elements is only 16 in the current version, additional elements could be connected in the same manner.

The cross-section of the sensor skin is shown in Fig.16. There are four conductive layers; the layers A, B, C, and D are the ground layer, the sensor/signal layer, the other sensor layer, and the power layer, respectively. The sensing chips are supplied with power from the layers A and D (the ground and power layers). These two layers also function as electrostatic shields. The layers A and B sandwich the soft insulator layer forming the capacitor C_1, and B and C sandwich the hard insulator layer forming C_2. The data packets are multi-hopped through the layer B (the signal layer) to the host computer.

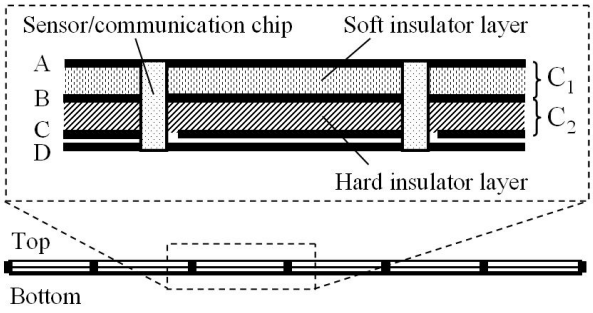

Figure 16: Cross-section of robot skin using sensor/communication chip. A: Ground layer, B: Sensor/signal layer, C: sensor layer, and D: Power layer.

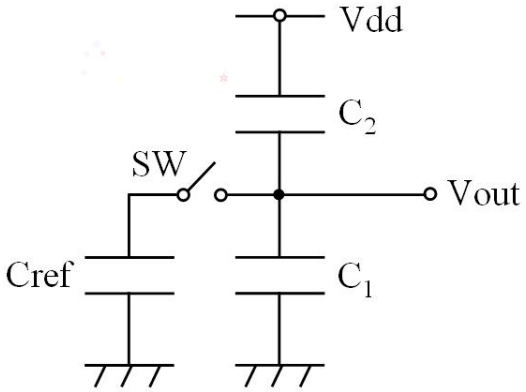

Figure 17: Equivalent circuit of measurement system.

3.2 Packets and operations

In the current version of the protocol, two kinds of packets, the data packet and the command packet, are employed. The packets are transmitted downstream (see Fig.15). The data packet contains the measured data and the coordinate of the sensor element, and the command packet contains the cue signal for the next chip to measure the capacitances of the sensor element.

The chip is on standby when there is no packet. In receiving the data packet, the chip transfers the identical packet to the downstream chip through the signal layer. On the other hand, in receiving the command packet, the chip executes the following two-step sequence. Firstly, the chip measures the capacitances C_n and sends the data packet containing the measured data to the downstream chip through the signal layer. Next, the chip generates and sends the command packet to the downstream chip. By the iteration of this process, the host computer can gather the data from the all sensor elements.

The most upstream chip connected to the sensor element with the coordinate (0, 3) alone executes the above sequence spontaneously at adequate intervals without waiting for the command packet.

3.3 Measurement method

Figure 17 shows the equivalent circuit of the measurement system. There is the reference capacitor C_{ref} inside the chip connected through the switch SW to the junction of the capacitors C_1 and C_2. The chip measures the divided voltage V_{out} between the power voltage V_{dd} and the ground. The divided voltages are represented as

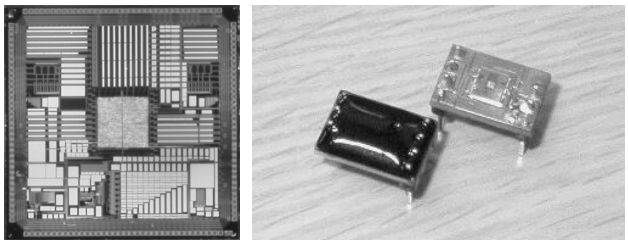

(a) (b)

Figure 18: (a) Closeup top view of fabricated CMOS LSI chip. The size of the chip is 5 x 5 sq mm. (b) CMOS LSI chip after bonding (right) and molding (left).

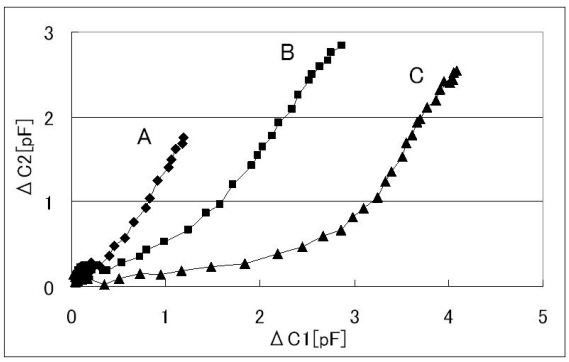

Figure 19: Experimental result on operation check of prototype of sensor/communication chip. Measured trajectories of capacitance variations for the stimulators with diameters of (A) 10 mm, (B) 20 mm, and (C) 40 mm.

$$V_{out}(\mathrm{OFF}) = \frac{C_2}{C_1+C_2}V_{dd} \quad (9)$$

$$V_{out}(\mathrm{ON}) = \frac{C_2}{C_1+C_2+C_{ref}}V_{dd} \quad (10)$$

where V_{out}(OFF) and V_{out}(ON) mean the voltages of the junction when the switch SW is off and on, respectively. The chip sends the values of V_{out}(OFF) and V_{out}(ON) after coding them by an A/D converter on the chip. We can know C_1 and C_2 by solving Eq.(9) and (10). The chip has initialization process before the measurement of V_{out}(OFF) and V_{out}(ON) in which the charges in C_1, C_2 and C_{ref} are all released.

3.4 Prototype of sensing chip

At the present stage, we have completed fabrication of the first prototype of CMOS LSI chip based on the 0.35 μm rule for the sensor/communication chip (Fig.18). While the size of the LSI chip is 5×5 mm^2, the total area of the analog-digital mixed circuits is within 1.5 mm^2. The operating frequency is 50 MHz. Each chip measures V_{out} with an 8-bit A/D converter and it has a function to transmit the data to the neighboring sensing chip.

We verified the chip could measure the capacitances of the sensor element and transmit data to a PC successfully. The data packets from the chip were received by a FPGA, and the data decoded by the FPGA were transferred to the PC via USB. In the experiment, three different acrylic circular cylinder stimulators A: D=10 mm, B: D=20 mm, and C: D=40 mm were vertically pressed at the center of the sensor element prototype by hand with force up to approximately 5 N in 1 s. In Fig.19, the $(\Delta C_1, \Delta C_2)$s during the motion are plotted. It is confirmed possible to discriminate the three stimulators by the sensor outputs.

We are in the process of arraying the sensor elements and connecting them by the fabricated LSI chips.

Acknowledgement

The authers thank Naoya Asamura, Tachio Yuasa, Mitsuhiro Hakozaki, Xinyu Wang, and Hiroto Itai (Cellcross Co., Ltd.) for their cooperation on fabricating and evaluating the prototype of the CMOS LSI chip, and providing ideas on device structures. We also thank Kosuke Ito (the University of Tokyo) for his contribution on conducting a part of the experiments.

References

[1] Y. Sakagami, R. Watanabe, C. Aoyama, S. Matsunaga, N. Higaki, and K. Fujimura. The intelligent asimo: Symtem overview and integration. *Proc. of the 2002 IEEE/RSJ International Conference on Intelligent Robots and Systems (IROS 2002)*, 3:2478–2483, 2002.

[2] K. Kaneko, F. Kanehiro, S. Kajita, H. Hirukawa, T. Kawasaki, M. Hirata, K. Akachi, and T. Isozumi. Humanoid robot HRP-2. *Proc. of the IEEE 2004 International Conference on Robotics and Automation (ICRA 2004)*, 2:1083–1090, 2004.

[3] T. Shibata, K. Wada, and K. Tanie. Tabulation and analysis of questionnaire results of subjective evaluation of seal robot in Japan, U.K., Sweden and Italy. *Proc. of the IEEE 2004 International Conference on Robotics and Automation (ICRA 2004)*, 2:1387–1392, 2004.

[4] M. Fujita. Aibo: Toward the era of digital creatures. *The International Journal of Robotics Research*, 20(10):781–794, 2001.

[5] M. H. Lee and H. R. Nicholls. Tactile sensing for mechatronics - a state of the art survey. *Mechatronics*, 9:1–31, 1999.

[6] E. S. Kolesar and C. S. Dyson. Object imaging with a piezoelectric robotic tactile sensor. *IEEE Journal of Microelectromechanical Systems*, 4:87–96, 1995.

[7] Y. Hoshino, M. Inaba, and H. Inoue. Model and processing of whole-body tactile sensor suit for human-robot contact interaction. *Proc. of the 1998 IEEE International Conference on Robotics and Automation (ICRA '98)*, pages 2281–2286, 1998.

[8] R. Kageyama, S. Kagami, M. Inaba, and H. Inoue. Development of soft and distributed tactile sensors and the application to a humanoid robot. *Proc. of the IEEE International Conference on Systems, Man, and Cybernetics*, 2:981–986, 1999.

[9] F. Castelli. An integrated tactile-thermal robot sensor with capacitive tactile array. *IEEE Transactions on Industry Applications*, 38(1):85–90, 2002.

[10] O. Kerpa, K. Weiss, and H. Worn. Development of a flexible tactile sensor system for a humanoid robot. *Proc. of the 2003 IEEE/RSJ International Conference on Intelligent Robots and Systems (IROS 2003)*, 1:1–6, 2003.

[11] M. Shimojo, A. Namiki, M. Ishikawa, R. Makino, and K. Mabuchi. A tactile sensor sheet using pressure conductive rubber with electrical-wires stitched method. *IEEE Sensors Journal*, 4:589–596, 2004.

[12] T. Hoshi and H. Shinoda. A tactile sensing element for a whole body. *Proc. of 36th International Symposium on Robotics (ISR 2005)*, 2005.

[13] Y. Makino, N. Asamura, and H. Shinoda. Multi primitive tactile display based on suction pressure control. *Proc. of IEEE 12th Symposium on Haptic Interfaces for Virtual Environment and Teleoperator Systems (Haptic Symposium 2004)*, pages 90–96, 2004.

[14] A. Okada, Y. Makino, and H. Shinoda. Cell bridge: A signal transmission element for constructing high density sensor networks. *Proc. of 2nd International Workshop on Networked Sensing Systems (INSS 2005)*, pages 180–185, 2005.

[15] G. R. Strobl. *The Physics of Polymers: Concepts for Understanding Their Structures and Behavior*. Springer, 1997.